APPARATUS AND DEMONSTRATION NOTES

Jeffrey S. Dunham, *Editor*
Department of Physics, Middlebury College, Middlebury, Vermont 05753

This department welcomes brief communications reporting new demonstrations, laboratory equipment, techniques, or materials of interest to teachers of physics. Notes on new applications of older apparatus, measurements supplementing data supplied by manufacturers, information which, while not new, is not generally known, procurement information, and news about apparatus under development may be suitable for publication in this section. Neither the *American Journal of Physics* nor the Editors assume responsibility for the correctness of the information presented. Submit materials to Jeffrey S. Dunham, *Editor*.

Jeffrey S. Dunham — New Apparatus and Demonstration Notes Editor for the *American Journal of Physics.*

I am pleased to announce that Jeffrey S. Dunham has agreed to take on the role of Apparatus and Demonstration Notes Editor of the *American Journal of Physics.* Dunham a Stanford Ph.D., has been at Middlebury College since 1983, where he is currently chair of the Department and carries out research in laser spectroscopy. Professor Dunham has been very successful at involving undergraduate students in his research; his most recent AJP publication [''High-resolution solar spectroscopy in the undergraduate physics laboratory,'' Am. J. Phys. **60** (7), 645–649 (1992)] carries the names of four Middlebury students as coauthors. His impressive Modern Physics Laboratory Manual is available on the web at www.middlebury.edu/~PHManual. Among other professional activities Dunham teaches a course entitled Chaos, Complexity, and Self-Organization for nonscience students.

Dunham succeeds Daryl W. Preston of California State University-Hayward, whose careful work as Apparatus and Demonstration Notes Editor has enriched the pages of this Journal for the last three years.

Robert H. Romer, *Editor*

Demonstrating optical saturation and velocity selection in rubidium vapor

K. Razdan
Department of Physics and Astronomy, University of Wisconsin–Stevens Point, Stevens Point, Wisconsin 54481

D. A. Van Baak
Department of Physics, Calvin College, Grand Rapids, Michigan 49546

(Received 8 July 1998; accepted 26 October 1998)

I. INTRODUCTION

The technique of saturated-absorption spectroscopy has been used to achieve spectral resolution below the ordinary limits of Doppler broadening, and the demonstration of this technique using 780-nm diode-laser excitation of rubidium vapor has become a classic student experiment in modern optics.[1] This note is intended to make the saturated-absorption technique more comprehensible to students by displaying and discussing two phenomena that make it possible. These are the ability of sufficiently strong light to saturate an atomic transition, and the possibility for narrow-band light to interact with only a part of the velocity distribution of a gaseous sample.

The two experimental demonstrations require, respectively, one and two narrow-band laser sources that are tunable over the atomic rubidium absorption lines near 780 (or 795) nm. It is the increasing availability, and decreasing cost, of such sources that make these demonstrations feasible. The sources may conveniently be free-running, or grating-tuned and spectrally narrowed, diode laser systems; power levels of a few milliwatts suffice for the experiments described here.

II. DISPLAYING SATURATION OF ATOMIC TRANSITIONS

We are conditioned to expect that a beam of light passing through a sample will be attenuated, perhaps in a frequency-dependent way, such that the sample can be characterized by a ''transmission coefficient'' T. Thus a neutral-density filter might have $T=0.25$ independent of the light's frequency, while a colored-glass filter might have T vary systematically with frequency. This section aims to show that, in contrast, atomic samples *cannot* be characterized by an ordinary transmission coefficient T, not even one with strong frequency dependence.

The experimental demonstration of this fact is very direct; it requires one tunable laser source whose beam reaches a detector after passing successively through two absorbers, one of them a neutral density filter, and the other an atomic vapor. The particular realization used here is shown in the inset of Fig. 1; it uses a 5-mW 780-nm diode-laser source and a fixed $T=0.50$ neutral-density filter to deliver, in a beam of size about $2\times 4\ \mathrm{mm}^2$, about 2.5 mW of linearly polarized light. The beam passes through the two samples of interest, a $T=0.13$ neutral-density filter and a 5-cm-long cell of room-temperature rubidium vapor, before reaching a silicon photodiode. The signal recorded is proportional to the power reaching the detector, and it is displayed in Fig. 1 as a function of the frequency of the diode-laser source.[2] The demonstration consists of comparing the signals obtained from two versions of the experiment, differing *only* in the order in which the light encounters the two absorbers. If the neutral-density filter's transmission T_{nd} is frequency independent, and if the rubidium vapor could be characterized by a frequency-dependent transmission coefficient $T_{\mathrm{Rb}}(f)$, then we would expect to obtain in the two cases the signals

$$P_1(f)=T_{\mathrm{Rb}}(f)T_{\mathrm{nd}}P_0(f), \quad P_2(f)=T_{\mathrm{nd}}T_{\mathrm{Rb}}(f)P_0(f), \quad (1)$$

where $P_0(f)$ is the output power of the diode laser as a function of frequency. Naturally we'd expect $P_1(f)=P_2(f)$; that is, we'd expect it not to matter in which order the light encounters the two absorbers.

But the data of Fig. 1 show that it *does* matter; the resonant absorption due to the 780-nm $5\,^2S_{1/2}-5\,^2P_{3/2}$ transitions in rubidium vapor thus cannot be characterized by an ordinary transmission coefficient $T_{\mathrm{Rb}}(f)$. In fact we see that the absorption dips due to atomic transitions in rubidium are deeper in the case in which the light first encounters the neutral-density filter. We are led to conclude that rubidium vapor will absorb a greater fraction of dim light than it will of bright light. If we consider a continuous variation of light intensity from zero intensity upwards, we could imagine a transmission coefficient defined in the low-intensity limit, but we see that the relative absorption decreases, and the absolute power absorbed and re-radiated becomes *saturated*, as the intensity reaches some characteristic level.

III. INTERPRETING SATURATION OF ATOMIC TRANSITIONS

We will now show that this ''saturation of absorption'' occurs for light bright enough to cause non-negligible depletion of the atomic ground-state population, and we will compute the scale of intensity required to exhibit this effect. To do this calculation, we introduce a two-level model of the sort Einstein used to understand the equilibrium of blackbody radiation with matter.[3] If we have ground-state atoms with population N_1, and excited-state atoms with population N_2, immersed in an isotropic, unpolarized radiation field of spectral energy density $u(\omega)$ (whose units are energy per unit volume per unit angular-frequency interval), then the populations change with time according to

$$\frac{dN_2}{dt}=+B_{21}N_1u(\omega_{12})-B_{12}N_2u(\omega_{12})-AN_2 \quad (2)$$

and

$$\frac{dN_1}{dt}=-B_{21}N_1u(\omega_{12})+B_{12}N_2u(\omega_{12})+AN_2. \quad (3)$$

Here $\omega_{12}=|(E_1-E_2)|/\hbar$ is the Bohr frequency of the transition between the states. The B_{21} terms give the rate of excitation of ground-state atoms to the excited state, while the B_{12} terms give the rate at which excited-state atoms are stimulated to make transitions to the ground state. Finally the terms in A give the rate of spontaneous decay of excited states. Standard calculations show that the mean lifetime of the excited-state atoms against spontaneous decay is $\tau=1/A$, and also show that the A and B coefficients are related by Einstein's results

$$A=(\hbar\omega_{12}^3/\pi^2c^3)B \quad (4)$$

with $B=B_{12}=B_{21}$.

Now if the sample is illuminated by a chosen spectral-density function $u(\omega)$, the steady-state solutions of (2) and (3) will obey the relationship

$$\frac{N_2}{N_1}=\frac{Bu(\omega_{12})}{Bu(\omega_{12})+A}. \quad (5)$$

Depending on the relative size of the two terms in the denominator, this fraction has two interesting limiting cases. If the excitation is *weak*, the second term dominates, and (5) gives

$$\frac{N_2}{N_1}\approx\frac{B}{A}u(\omega_{12}), \quad (6)$$

so that the degree of excitation is directly proportional to the strength of the exciting fields; this is the linear regime, in which the sample *can* be characterized by an ordinary transmission coefficient.

If, on the other hand, the excitation is *strong*, then the first term in the denominator in (5) dominates, and we have

$$\frac{N_2}{N_1}\to 1,$$

which shows that a strong enough field will tend to equalize the ground-and excited-state populations, so that nearly half of all the atoms are in the excited state. Under these conditions, the sample's absorption drops nearly to zero (since stimulated emission will restore to the radiation field nearly as many photons as absorption removes), and the sample can certainly not be characterized by its weak-field transmission coefficient.

The boundary between the weak- and strong-field regimes may conveniently be located where the two terms in the denominator in (5) are equal; this gives for the onset of saturation the condition

$$u_{\mathrm{sat}}(\omega_{12})=\frac{A}{B}=\frac{\hbar\omega_{12}^3}{\pi^2c^3}=\frac{4h}{\lambda^3}, \quad (7)$$

where λ is the wavelength of the light resonant with the transition. According to this criterion, the onset of saturation

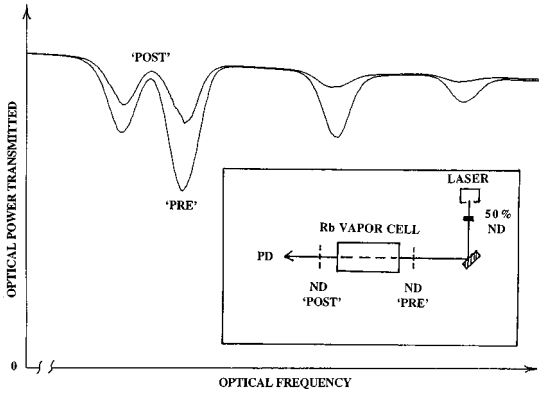

Fig. 1. Graphs of optical power transmitted through the combination of a rubidium-vapor absorption cell and a 13%-transmission neutral-density filter, plotted as a function of optical frequency over a range of about 10 GHz near the 780-nm rubidium resonance line. The inset shows the arrangement of a tunable diode-laser source, a fixed 50%-transmission neutral-density filter, the vapor cell, the photodetector PD, and the two possible positions for the 13%-transmission neutral-density filter. The curves shown have a baseline of zero optical power, and the two graphs labeled ''pre'' and ''post'' correspond to positioning the 13%-transmission filter before, or after, the rubidium cell.

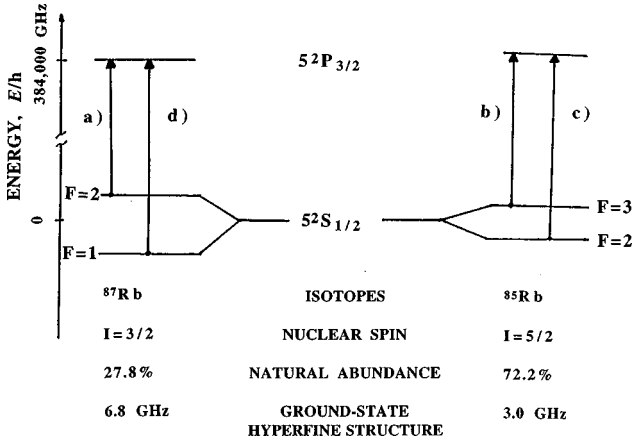

Fig. 2. Energy-level diagram for the 780-nm resonance transitions in atomic rubidium. The ground-state hyperfine splittings of 6.8 and 3.0 GHz for rubidium-87 and -85 are indicated; the excited-state hyperfine splittings (all less than 0.5 GHz) have been omitted. The four transitions have been labeled a, b, c, d in order of increasing optical frequency.

corresponds to having one-third of the atoms in the excited state, and two-thirds in the ground state.

Now in isotropic radiation fields, the rate at which energy crosses any surface gives a spectral density of irradiance (with units of power per unit area per unit angular-frequency interval) related to the spectral density of energy by

$$I(\omega)=\tfrac{1}{4}cu(\omega), \tag{8}$$

so we can define a saturation value of irradiance as

$$I_{\mathrm{sat}}(\omega)=\frac{c}{4}u_{\mathrm{sat}}(\omega)=\frac{hc}{\lambda^3}. \tag{9}$$

This is still a spectral density, but it can be connected to the ordinary irradiance I (power per unit area) of an approximately monochromatic beam by noting that the light beam would have nearly the same effects on the atoms if its energy were spread out in frequency over the natural linewidth $\Delta\omega=1/\tau$ of the atomic transition. This would give a spectral density

$$I(\omega)=\frac{I}{\Delta\omega}, \tag{10}$$

so the saturation irradiance, I_{sat}, is finally

$$I_{\mathrm{sat}}=I_{\mathrm{sat}}(\omega)\Delta\omega=\frac{hc}{\lambda^3}\frac{1}{\tau}. \tag{11}$$

This result differs from the more detailed calculation quoted by Metcalf[4] only by a factor of $(\pi/3)$, which is better agreement than we might expect, given the cavalier treatment of polarization and directional effects in the derivation above.

The rubidium atomic transition in question has $\lambda=780\,\mathrm{nm}$, and the upper state has $\tau=26.6\,\mathrm{ns}$,[5] so we compute the saturation irradiance to be

$$I_{\mathrm{sat}}=16.0\,\mathrm{W/m^2}=1.60\,\mathrm{mW/cm^2}. \tag{12}$$

In the experimental setup shown, a laser with output power 5.0 mW, attenuated to 2.5 mW by a fixed $T=0.50$ neutral-density filter, was collimated into a parallel beam of approximate dimensions $2\times4\,\mathrm{mm^2}$, so the beam used in the experiment had an irradiance of about

$$(2.5\,\mathrm{mW})/(0.2\times0.4\,\mathrm{cm^2})=31\,\mathrm{mW/cm^2}. \tag{13}$$

The beam encountering the rubidium vapor had an irradiance that depended on the position of the 13% neutral-density filter; in the ''pre'' position, the irradiance was about 4 $\mathrm{mW/cm^2}$, while in the ''post'' position, the irradiance was the full 31 $\mathrm{mW/cm^2}$. These two irradiances are, respectively, on the edge of, and well into, the saturation region derived theoretically above, and are manifestly intense enough to account for the saturation phenomena displayed in Fig. 1. Detailed quantitative comparison is much harder, and is not attempted here; one of the many difficulties is the transverse profile of the laser beam, which means that absorption in the laser beam's center may become saturated while absorption in the fringes of the beam is still in the linear regime. But we have shown experimentally that saturation is an empirical fact, and we've shown theoretically the intensity scale required to exhibit this effect.

IV. DEMONSTRATING VELOCITY SELECTION IN ABSORPTION

Our goal of exhibiting velocity-selective effects in the interaction of light with matter, and the need to understand the structure exhibited by the graphs in Fig. 1, require that we introduce some details of the energy-level structure lying behind the 780-nm transition in atomic rubidium. This is displayed in Fig. 2, which shows the existence of two isotopes in rubidium and the splitting of the electronic ground state of each isotope by hyperfine structure. Ignoring the smaller hyperfine structure of the excited state, this isotope and hyperfine structure allows four different transition frequencies within the 780-nm resonance line, and these correspond to the four absorption dips exhibited in the data of Fig.

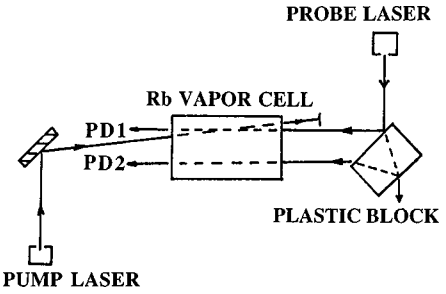

Fig. 3. Experimental arrangement for demonstrating velocity-selective population redistribution in rubidium vapor. The probe laser is continually scanned in frequency, and is used to form two weak probe beams passing through the rubidium-vapor absorption cell; the pump laser is held fixed in frequency, and sends a counterpropagating strong beam through the rubidium cell, overlapping there with only one of the probe beams. The experimental differential-transmission signal is derived from the difference in the optical power of the two probe beams, as measured by photodetectors PD1 and PD2.

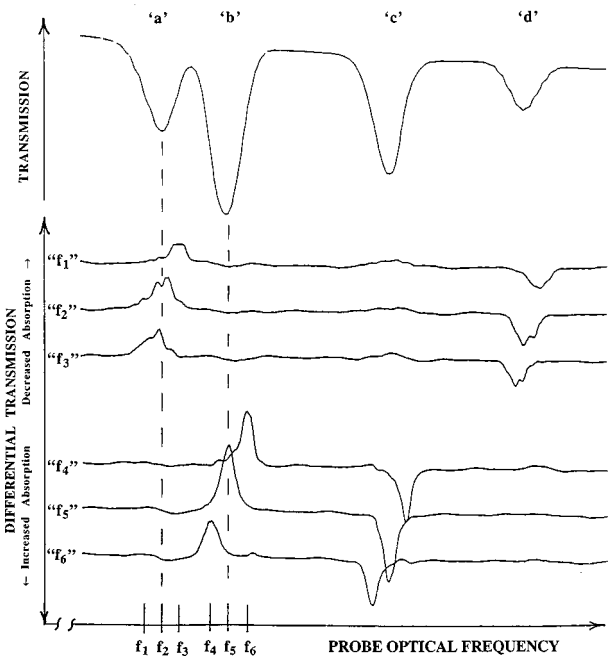

Fig. 4. Signals observed as a function of the frequency of the scanned probe laser. The uppermost trace shows the transmission signal obtained with a single probe beam (and with no pump beam); the six lower traces all show differential transmission measured using both probe beams (with the pump beam present). Traces ''f_1'' through ''f_6'' (with their zeros displaced vertically) show the results of setting the pump-laser frequency successively to the six optical frequencies labeled f_1 through f_6 on the optical frequency scale shown.

1. For reference, the optical frequencies involved are all in the neighborhood of 384 000 GHz, and the width of the frequency scan in Fig. 1 is of the order of 10 GHz. The nonzero width of the four absorption dips is due largely to the room-temperature Doppler broadening of the transitions (full width at half-maximum calculated to be about 0.5 GHz), though there is some broadening due to upper-state hyperfine structure (0.1–0.3 GHz), and the linewidth of the diode-laser radiation ($<$0.1 GHz).

We now introduce a second experimental demonstration, aimed at direct confirmation of the role of atomic velocities in causing the Doppler broadening exhibited in Fig. 1, and also confirming that Doppler broadening can in fact be surmounted. The demonstration discussed here requires two independently tunable laser sources, but it allows the study of phenomena not visible in the ordinary one-laser demonstration of saturated-absorption spectroscopy. The role of the two lasers is different, so the technique also illustrates very concretely the important pump–probe technique useful in so many forms in modern spectroscopy.[6] The output of one of the lasers is divided into two weak beams, both passing through the sample and each independently monitored by photodiodes; this laser is continually scanned over the rubidium resonances, and each beam serves as a ''probe'' of the absorption of light by the atoms in the vapor. The other laser provides a single, stronger, ''pump'' beam, and this is sent through the sample too, but in the opposite direction, and overlapping with only one of the ''probe'' beams in the vapor cell.[7] The goal is to use the two probe beams differentially, and thus to see what difference the pump beam causes in the absorption due to the atoms it illuminates. The geometry used is shown in Fig. 3; in practice, the two parallel and weak ($\ll$1 mW) probe beams are derived from the Fresnel reflections at the two faces of an (uncoated) thick plastic block, while the pump beam comes directly from the other diode laser and has a power of order 5 mW; all the beams have the same linear polarization.

In the absence of any pump beam, each probe beam suffers absorption as a function of frequency in the fashion illustrated in Fig. 1; the difference in the two probe beams' absorption is negligible, and this real-time difference signal provides a baseline against which the effects of the pump beam will be visible. We then introduce the pump beam at a fixed (unscanned) frequency, and look for its effect on the differential transmission signal. The effects we see are illustrated in Fig. 4, and they depend on the presence, and the frequency, of the pump beam. The frequency to which the pump laser is tuned can be easily established in a separate fluorescence experiment, and this allows the pump beam to be set (for instance) to one of the six optical frequencies labeled f_1–f_6 on the optical frequency scale in Fig. 4. For example, a first scan labeled ''f_1'' is obtained with the pump laser set to frequency f_1, *below* the central frequency of component ''a'' of the four-line absorption structure of the rubidium resonance line. This scan displays nonzero differential-transmission features, as shown in the trace labeled ''f_1'' in Fig. 4.

The features of this trace are very instructive. We see first of all that there is no differential transmission in either of the two components ''b'' or ''c'' in the pattern, and we ascribe this to the isotopic composition of rubidium. In scan ''f_1'' the pump laser, set to optical frequency f_1, is interacting only with rubidium-87 atoms; so the components ''b'' and ''c,'' due to rubidium-85 atoms, are entirely unaffected.

In the differential-transmission signals, we next see that component ''a'' of the four-line pattern *is* affected, but that the effect comes *not* at the optical frequency f_1 of the pump laser, but rather at an optical frequency *above* the central frequency of component ''a.'' This feature, shown in scan ''f_1'' of Fig. 4, then moves *down* in optical frequency as the pump laser frequency is moved *up* in scans ''f_2'' and ''f_3.'' This is direct evidence of the role of atomic velocities in creating the Doppler-broadened profile exhibited by feature ''a.'' The reason the feature in question appears at all is that the pump beam, at one fixed frequency f_1, interacts only

with those rubidium-87 atoms having the longitudinal velocity component required to bring them into resonance with the pump laser. In trace ''f_1,'' where the pump laser is tuned *below* resonance, the only atoms that interact with the pump laser are those that are moving *toward* the pump laser, at the velocity required to produce the necessary Doppler shift in frequency. Furthermore, the atoms that are thus affected by the pump laser are removed from the ground-state population, since they have become part of the excited-state population distribution. Because the pump beam has an intensity well into the saturation regime, this causes a non-negligible deficiency of atoms in one particular velocity class in the population of ground-state atoms;[8] this deficiency is revealed as decreased absorption of light in the probe beam headed toward detector PD1. Since the atoms that are involved are moving toward the pump laser, however, they are moving *away* from the probe laser beams; thus because of the Doppler effect their effects are seen when the probe laser is tuned *above* the resonant frequency of atoms at rest.

Further evidence for the velocity selectivity of this process comes from the *widths* of the features shown in scans ''f_1,'' etc. The pump laser is interacting with only one velocity class of atoms, so that the differential signal revealed by the probe laser will also be due to one velocity class. Thus the absorption features shown in scans ''f_1''–''f_6'' are not Doppler broadened; rather, they reveal the absorption spectrum due to velocity-selected atoms. Since the width of these absorption features is smaller than the ordinary Doppler width, this technique permits spectroscopy beyond the resolution limit ordinarily imposed by Doppler broadening. This is one of the main purposes of the saturated-absorption technique, and its utility is revealed in this example by the substructure clearly visible in scan ''f_2'' of Fig. 4, which displays incipient resolution of the hyperfine structure of the *excited* state of the rubidium 780-nm transition.

The third feature of interest in Fig. 4 is the ''hyperfine pumping'' exhibited in the data. When the pump laser is set to optical frequency f_2, near the center of component ''a'' of the four-line pattern, the expected decrease in absorption in this component is seen, and it is seen at optical frequency f_2. The unexpected thing is the *increase* in absorption that can be seen at a quite different frequency, near the center of component ''d'' of the four-line pattern. This effect can be understood by reference to the energy-level diagram of Fig. 2: When the pump laser is tuned to frequency f_2, it is exciting (only) rubidium-87 atoms, and (only) those in the $F=2$ hyperfine level of the ground state, to the excited state. These atoms are allowed to decay back either to the $F=2$, or to the $F=1$, hyperfine level of the ground state. Not only does the steady presence of the pump laser cause a steady-state deficiency of atoms in the $F=2$ substate of the ground state; it also simultaneously causes an *excess* of atoms in the $F=1$ substate of the ground state. This excess is displayed as increased absorption in component ''d'' of the four-line pattern, since this marks the optical frequency at which the probe laser interacts with the $F=1$ substate of the ground state.

This hyperfine pumping is velocity selective, as comparisons of the features of scans ''f_1''–''f_3'' reveal; it is also isotope selective. Scans ''f_4''–''f_6'' are obtained with the pump laser set in the vicinity of component ''b,'' thereby depleting the $F=3$ hyperfine level of rubidium-85; the results show up as decreased absorption near component ''b,'' increased absorption near component ''c,'' and no effect at all in the two outer components due to rubidium-87.

V. CONCLUSIONS

The two experimental demonstrations discussed here offer students the opportunity to see the separate effects of optical saturation and of velocity selectivity, illustrated in experiments of maximal clarity and minimal complexity. We suggest that they should be useful introductory exercises for students attempting to understand the valuable technique of Doppler-free saturated-absorption spectroscopy, or indeed any of the range of pump–probe spectroscopies widely used in modern atomic and molecular physics.

ACKNOWLEDGMENTS

This work was supported in part by the National Science Foundation under Grant No. DUE-9455064. KR acknowledges the University of Wisconsin–Stevens Point for awarding a sabbatical leave and a laboratory modernization grant, and the Calvin College Physics Department for providing hospitality during the sabbatical.

[1]John R. Brandenberger, ''Saturated Absorption Laser Spectroscopy,'' in *Lasers and Modern Optics in Undergraduate Physics* (Lawrence U.P., Appleton, WI, 1989); Daryl W. Preston, ''New problems: Doppler-free saturated absorption: Laser spectroscopy,'' Am. J. Phys. **64**, 1432–1436 (1996).

[2]The diode-laser source used was a Sharp LT022MC device chosen for operation at 780 nm. It was held at constant temperature by methods described in D. A. Van Baak, ''Temperature servomechanisms using thermoelectric modules,'' Am. J. Phys. **60**, 803–815 (1992); it was tuned in frequency by slow variation of its operating current, as described in Sec. III of D. A. Van Baak, ''Resonant Faraday rotation as a probe of atomic dispersion,'' *ibid.* **64**, 724–735 (1996). Such a ''free-running'' diode-laser source may be expected to have a spectral linewidth of about 40 MHz, much smaller than the Doppler broadening of about 500 MHz displayed in Fig. 1.

[3]See, for example, David J. Griffiths, *Introduction to Quantum Mechanics* (Prentice–Hall, Englewood Cliffs, NJ, 1995), Chap. 9.3, pp. 311–319.

[4]Harold Metcalf and Peter van der Straten, ''Cooling and trapping of neutral atoms,'' Phys. Rep. **224**, 203–286 (1994).

[5]U. Volz and H. Schmoranzer, ''Precision Lifetime Measurements on Alkali Atoms and on Helium by Beam-Gas-Laser Spectroscopy,'' Phys. Scr. **T65**, 48–56 (1996).

[6]The pump–probe technique is described in many places, including Wolfgang Demtroder, *Laser Spectroscopy* (Springer, Berlin, 1996), pp. 444–487, 640–646, and 715–719; Marc D. Levenson and Satoru S. Kano, *Introduction to Nonlinear Laser Spectroscopy* (Academic, New York, 1988), Chap. 3, pp. 78–127.

[7]The probe beam used was derived from a continually scanned ''free-running'' diode laser, just as in Sec. II; the pump beam used came from a New Focus model 6200 grating-tuned diode-laser system delivering fixed-frequency light of spectral linewidth of only a few MHz. Use of spectrally narrowed sources for both pump and probe would improve the spectral resolution displayed in Fig. 4; use of free-running lasers for both sources would lower the costs involved. One approach to grating-tuned diode-laser systems is described in K. B. MacAdam, A. Steinbach, and C. Wieman, ''A narrow-band tunable diode laser with grating feedback, and a saturated absorption spectrometer for Cs and Rb,'' Am. J. Phys. **60**, 1098–1111 (1992).

[8]Causing such a deficiency in the population of one velocity class is often called ''burning a hole in the velocity distribution.''

A device for demonstrating interference fringes and electro-optic effect in crystals

Leonid A. Ageev and Vladimir D. Yegorenkov
Department of Physics, Kharkov State University, 4 Svobody Square, 310077, Kharkov, Ukraine

(Received 17 April 1998; accepted 26 October 1998)

From the pioneering effort by Talbot[1] to the present, the interference fringes formed by polarized convergent light in crystals[2,3] have been observed in a microscope fitted with polarizing attachments. The demonstration of interference patterns to a large audience can be accomplished by optical or TV projection onto a screen. Here we report a simple optical device (Fig. 1) which gives an immediate projection of bright patterns of large dimensions. To achieve this result, a wide-angle, large-aperture Erfle eyepiece is used. In our device the optical array of the Erfle eyepiece serves not as an eyepiece, but to focus a beam of light on a crystal and to project a nonlocalized interference pattern onto a distant screen.

The device includes a source of light S (an incandescent lamp, 6 V, 6 W), an Erfle eyepiece with the elements labeled $L_1L_2L_3$ (similar to one available from Edmund Scientific[4]), two polarizers (polaroids) P_1 and P_2, and a Pockels cell made of a DKDP single crystal (potassium dihydrogen phosphate doped with deuterium). The cell with the dimensions $1\times1\times1$ cm is placed between the polarizers. The length of the eyepiece cover is 40 mm, the diameters of its apertures are denoted with the sign ''$\varnothing$'' and they are equal to 26 and 30 mm. The light source is located on the output side of the eyepiece. Figure 1 also shows other necessary dimensions.

The eyepiece builds up a convergent beam of light that passes through the polarizer P_1 and is focused inside the crystal. The Pockels cell is homebuilt. The DKDP crystal has been donated to us by colleagues from the Scientific Technical Complex ''Institute for Single Crystals,'' National Academy of Sciences of Ukraine, Kharkov, Ukraine. The cell is made as follows. The crystal is cut perpendicular to its optic axis. Transparent conducting CuI films[5] approximately 100 nm thick are formed on its polished faces. We have prepared CuI films in two stages. First, a copper film approximately 25 nm thick is made using the vacuum deposition technique. This thickness value has been evaluated from the mass of the evaporated copper. The Cu film obtained is transformed into a transparent CuI film in iodine vapor. The iodine vapor is obtained at room temperature from a small piece of crystalline iodine placed on the bottom of a closed desiccator. During the iodination process, the crystal rests on the desiccator table. The process is terminated when the film is completely transparent, the control being performed visually. The CuI films may also be prepared with direct vacuum deposition of the ready-made CuI compound. After the CuI films are ready, the Pockels cell is placed into the device. A dc potential difference is applied across the crystal resulting in a dc electric field strength directed along the optic axis of the crystal. The power supply should give a smooth dc potential difference variable between 0 and 15 kV.

The divergent beam of light leaving the crystal passes through the polarizer P_2 and hits a screen placed at a dis-

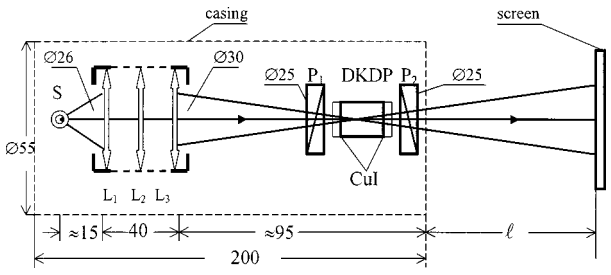

Fig. 1. Design of the device. All dimensions are in mm.

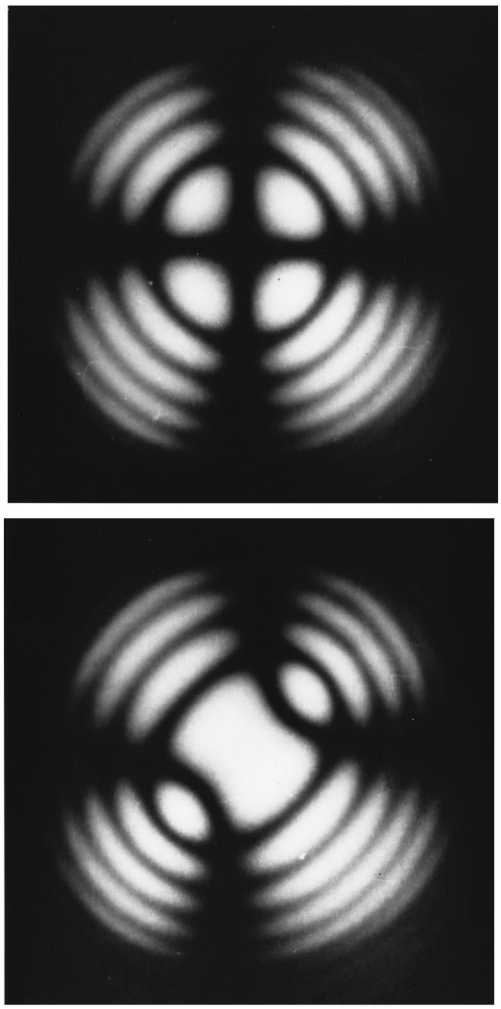

Fig. 2. Interference patterns with crossed polarizers: (a) potential difference switched off ($V=0$), (b) potential difference switched on ($V=6$ kV).

tance l from the output face of the device which is not less than 0.5 m. On the screen, which may be placed at any distance exceeding 0.5 m, an interference pattern is observed whose dimensions depend upon l. For example, at $l=1.5\,\mathrm{m}$ the diameter of the pattern is 0.5 m. The brightness is sufficient for demonstration on the walls or the ceiling of a large darkened room.

When the potential difference is switched off and the polarizers are crossed, a pattern of colored interference rings is observed with a dark cross, often referred to as the ''brushes'' [Fig. 2(a)]. As the potential difference V is increased, the pattern gradually changes until it has two ''eyes;'' these are associated with a biaxial crystal cut perpendicular to the bisector of the axes. In the device one employs a DKDP crystal possessing the $\overline{4}2m$ symmetry group. The matrix of the electro-optic effect for these crystals contains the electro-optic coefficient r_{63}. When an electric field $\mathbf{E}_z$ directed along the optic axis z is applied, then the index ellipsoid assumes the form[6]

$$\frac{x^2+y^2}{n_o^2}+\frac{z^2}{n_e^2}+2r_{63}E_z xy=1, \tag{1}$$

where n_o, n_e are the principal values of refraction indices for the ordinary and extraordinary waves. From this equation one finds the refractive indices (half-axes of the index ellipsoid which now relates to a biaxial crystal):

$$\begin{aligned} n_{x'}&=n_o-\frac{n_o^3}{2}r_{63}E_z,\\ n_{y'}&=n_o+\frac{n_o^3}{2}r_{63}E_z,\\ n_z&=n_e, \end{aligned} \tag{2}$$

where x', y' are the axes x and y, rotated around the z axis over the angle 45°.

The quantitative evaluation of changes observed in the interference pattern may be made if the dispersions of the refractive indices $n_o(\lambda), n_e(\lambda)$ and of the electro-optic coefficient $r_{63}(\lambda)$ are known.[6]

Thus we are able to show to a large audience a continuously changing set of interference patterns related to a smooth transition from a single-axis crystal to a double-axis one. Figure 2(b) shows the pattern at $V=6\,\mathrm{kV}$.

This device makes it possible to demonstrate the interference fringes of convergent polarized beams in crystals at any orientation of the crystal axes with respect to the device's optic axis. It is used for lecture demonstrations concerning optical phenomena associated with the structure of crystals, with the longitudinal Pockels effect, as well as in a laboratory to study the effect. In the laboratory application the light propagating along the optic axis of the device hits the entrance slit of a monochromator. At the exit of the monochromator the dependence of the transmitted light intensity I on the potential difference V applied across the crystal is measured for different wavelengths λ, i.e., the dependence

$$I=I_0\sin^2(\pi V/2V_{1/2}), \tag{3}$$

where $V_{1/2}=\lambda/2n_o^3r_{63}$ is the half-wave potential difference at which the phase shift between the two orthogonal-polarized waves inside the crystal is π. When the wavelength λ is given, the maximum of $I(V)$ yields the half-wave potential difference $V_{1/2}$, whence one may find the parameter r_{63} if the n_o value is known.

When a brighter source is used (e.g., a halogen lamp) and the potential difference values are programmable, this device can also be used to generate dynamic light effects for shows in large halls.

[1]Jon Darius, *Beyond Vision* (Oxford U.P., Oxford, New York, 1984), p. 12.
[2]Max Born and Emil Wolf, *Principles of Optics* (Pergamon, Tarrytown, NY, 1980), 6th ed., pp. 701–702.
[3]Francis A. Jenkins and Harold E. White, *Fundamentals of Optics* (McGraw–Hill, New York, 1985), 4th ed., p. 576.
[4]Edmund Scientific, Optics and Optical Instruments Catalogue N981B 1998, p. 3, Model #D41,347.
[5]Yoshihiro Kokubun, Hideo Watanabe, and Masanobu Wada, ''Electrical Properties of CuI Thin Films,'' Jpn. J. Appl. Phys. **10** (7), 864–867 (1971).
[6]Amnon Yariv and Pochi Yeh, *Optical Waves in Crystals* (Wiley, New York, 1984), pp. 229–234.

Visualization of high frequency modes of vibrating bells using high sensitive holographic plates

Hugues Mesnil, Yves Colombe, Louis-Nicolas Hallez, Vincent Gibiat, and Holger Vach[a)]
Laboratoire d'Optique Quantique du CNRS, Ecole Polytechnique, 91128 Palaiseau Cedex, France

(Received 24 July 1998; accepted 25 November 1998)

Recently, we showed the feasibility of studying vibrational modes of a bell in an undergraduate lab class using holography with standard lab class material, for instance HeNe lasers.[1] We employed both acoustic and mechanical excitation of the bells. Due to the ω^{-2} dependence of the vibrational amplitude on excitation frequency ω, we were limited to the first two resonance frequencies, 363 and 371 Hz, of our bell when using acoustic excitation with a loud-

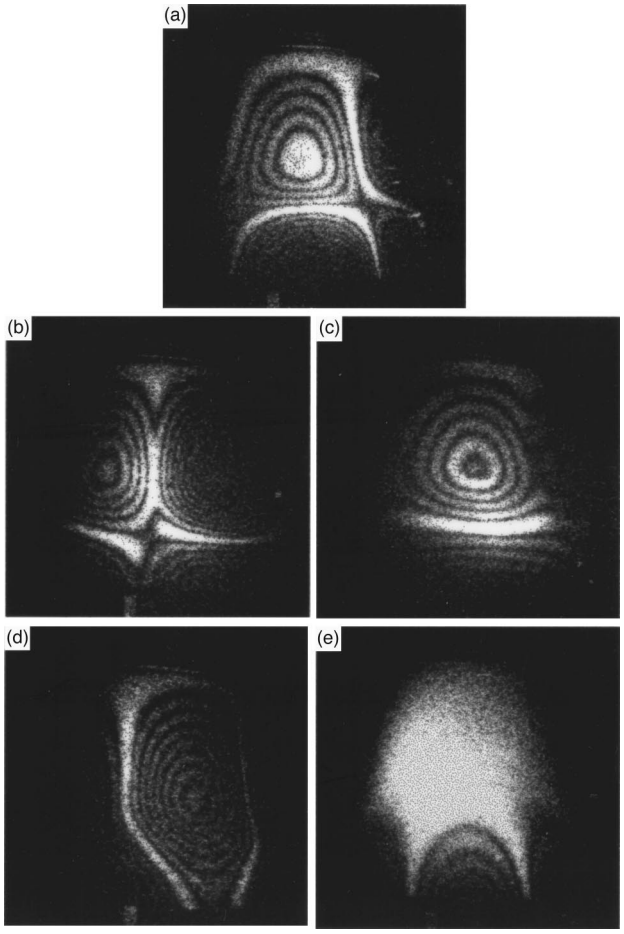

Fig. 1. Photographs of the holograms recorded at vibrational frequencies of (a) 1830 Hz, (b) 1918 Hz, (c) 1921 Hz, (d) 2075 Hz, and (e) 2575 Hz tentatively identified as modes (m,n), where $2m$ is the number of nodal lines perpendicular to the main circles and n is the number of nodal circles: (a) (3,1), (b) (3,1#), (c) (3,1#), and (e) (4,1), respectively. The modes shown in (b) and (c) are degenerate. The mode displayed in (d) has not been identified yet.

speaker. Using a mechanical shaker, on the other hand, we could also excite higher frequency modes of the bell. However, it was impossible to record holograms for those modes since the mechanical excitation caused a considerable amount of stray vibration of the holographic table. This problem was especially severe since the holographic plates we used (AGFA 8E75HD) were not very light sensitive, i.e., for most holograms we needed exposure times of about 90 s.

AGFA stopped its production of holographic plates a couple of months ago. For our lab classes, we are now using two different types of holographic plates: The first ones are plates from the company ABSYS with the reference number BB-640 which, due to their extremely small grain size, lead to very high quality holograms, but only for exposure times that are typically still three times longer than those for the former AGFA plates. The second kind of plates are produced by Kodak (Kodak SO-253) and can be characterized by a relatively large grain size resulting in a very sensitive recording material, i.e., typical exposure times might be up to 25 times shorter than with AGFA plates.

The use of these high sensitive Kodak plates permits us to reduce the recording times for the vibrating bells to as little as 3 s. Consequently, our experiments are much less sensitive to stray vibrations of our holographic setup, and we are now able to study the high vibrational modes of our bell as shown in Fig. 1.

We found that this development is very exciting for our students since they are now able to perform experiments within their regular lab class that were so far reserved to professional acoustic laboratories.[2,3]

ACKNOWLEDGMENT

We'd like to address our special thanks to the ''Centre de Travaux Experimentaux'' of the Physics Department of the Ecole Polytechnique where the hologrames were recorded.

[a]Electronic mail: vach@leonardo.polytechnique.fr

[1]K. Menou, B. Audit, X. Boutillon, and H. Vach, ''Holographic study of a vibrating bell,'' Am. J. Phys. **66**, 380–385 (1998).

[2]N. H. Fletcher and T. D. Rossing, *The Physics of Musical Instruments* (Springer-Verlag, New York, 1991), pp. 577–605.

[3]T. D. Rossing, R. Perrin, H. J. Sathoff, and R. W. Peterson, ''Vibrational modes of a tuned handbell,'' J. Acoust. Soc. Am. **76**, 1263–1267 (1984).

Interference of laser light scattered from a ''dusty'' plane mirror

Javier González, Anayeli Bravo, and Karol Juárez

Plantel Nopala, Colegio de Bachilleres del Estado de Hidalgo, Apartado Postal 95, Huichapan, Hidalgo. México, 42400

(Received 8 July 1998; accepted 12 November 1998)

Interesting and simple interference experiments using laser beams have been reported in the literature.[1–6] In these papers light interference is obtained using glass plates,[1] film plates,[2] cylindrical glasses,[3] computer punchcards,[4] lenses,[5] and microscope slide glass covers.[6]

This paper describes a simple interference experiment in scattered light using a ''dusty'' plane back-silvered mirror, a screen, and a laser. The interference pattern results from light scattering from the front-surface dust particles and the back-silvered surface. The oldest experiments with scattered light,

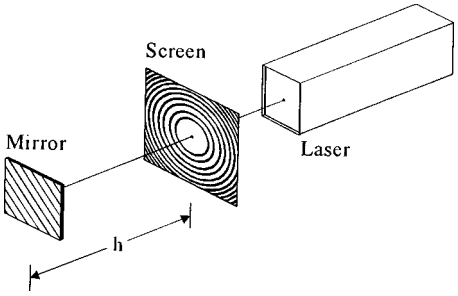

Fig. 1. Experimental arrangement for interference with a plane mirror and laser.

observed by Newton[7] and explained later by Young,[8] are presented by Walker[9] and in a review paper by de Witte.[10]

A clean plane mirror can be adapted to a ''dusty'' mirror using chalk dust,[10] or by rubbing its surface with children's modeling clay.[11] Both produce the same interference effect, and the only difference is that with modeling clay a brighter image is obtained.

The beam from a He–Ne laser first passes without diffracting through a hole in a screen, which is mounted in front of the laser. It shines perpendicular to a dusty plane mirror as shown in Fig. 1.

The interference of scattered light from a dusty plane mirror with conventional light sources is well explained by Walker,[9] de Witte,[10] and Pohl.[11] In the case of parallel light falling on the mirror, the interference effect is explained by de Witte[10] in the following way: ''Each scattering particle of the dusty mirror surface and its reflection together act as a double source of scattered light. Interference from each twin source produces the basic fringe pattern.'' For the laser, the beam of light is parallel rays with high accuracy.

Thus, laser light reflected and scattered from the dusty mirror produces a beautiful interference pattern on the screen. This pattern consists of alternating bright and dark concentric, circular rings around the screen hole. The bright reflected image at the center is the point of zeroth-order interference. When the mirror is slightly tilted, the rings remain concentric, but they seem to open up from the center, where the zeroth-order changes alternately from bright to dark.

Formulas for the interference of scattered light by reflection from a plane dusty mirror are given by de Witte.[10] For normal incidence of parallel light the angular coordinate β, where constructive interference occurs, is described by de Witte[10] as

$$\sin^2 \beta \approx (\mu/\tau) n\lambda, \tag{1}$$

where τ is the thickness of the mirror, μ is the refractive index of the glass ($\mu \approx 1.5$), n is the bright ring order number ($n=0,1,3,...$), λ is the laser wavelength ($\lambda = 6.328 \times 10^{-7}$ m), and β is the angular coordinate of the nth bright ring measured relative to the incident laser beam.

The radius r of the interference bright rings and the distance h of the screen to the mirror are related by

$$\tan \beta = r/h, \tag{2}$$

and, for small emerging angles β,

$$\sin \beta \approx r/h. \tag{3}$$

Using Eqs. (1) and (3), we obtain

$$r^2 \approx (\mu/\tau) n\lambda h^2. \tag{4}$$

Using different thickness mirrors (for example, $\tau = 2.3 \times 10^{-3}$ m and $\tau = 4.1 \times 10^{-3}$ m), and different distances h (for example $h = 1.6$ m and $h = 0.9$ m), we have obtained average radii (r) for several ring orders (n) that are in very good agreement with Eq. (4).

This demonstration is easily reproducible, and it is illustrative of light scattering and interference.

ACKNOWLEDGMENTS

The authors would like to thank Dr. J. Cantó, E. Guerrero, C. Uribe, H. Higgins, and V. García for their suggestions, and Dr. R. Ortega for the use of his He–Ne laser. Also thanks to A. García for the drawing.

[1]G. A. Woolsey, ''Laser optics experiments with glass plates and modified Jamin interferometer,'' Am. J. Phys. **41**, 255–259 (1973).
[2]C. Pontiggia and L. Zefiro, ''An experiment on interference in scattered light,'' Am. J. Phys. **42**, 692–694 (1974).
[3]W. C. Maddox, B. W. Koehn, F. H. Stout, D. A. Ball, and R. L. Chaplin, ''Interference pattern of a cylindrical glass tube,'' Am. J. Phys. **44**, 387–388 (1976).
[4]M. J. Moloney, ''Laser interference experiment using punchcard slits,'' Am. J. Phys. **51**, 468 (1983).
[5]A. F. Leung and J. E. Lee, ''Newton's rings: A classroom demonstration with a He–Ne laser,'' Am. J. Phys. **59**, 662–664 (1991).
[6]S. K. Derby and H. Kruglak, ''Interference finges with a laser,'' Am. J. Phys. **64**, 508 (1996).
[7]I. Newton, *Opticks* (Dover, New York, 1952), p. 289.
[8]T. Young, ''The theory of light and colors,'' Philos. Trans. R. Soc. London **1**, 41 (1802).
[9]J. Walker, *The Flying Circus of Physics* (Wiley, New York, 1977), p. 133.
[10]A. J. de Witte, ''Interference in scattered light,'' Am. J. Phys. **35**, 301–313 (1967).
[11]R. W. Pohl, ''Discovery of interference by Thomas Young,'' Am. J. Phys. **28**, 530–532 (1960).

PAULI TO SCHWINGER TO PURCELL

[Robert Kyhl] later reflected on the lengths to which [Rabi] had gone. Just before the war ended, the noted physicist Wolfgang Pauli was brought in to lecture on modern quantum mechanics. ''A couple of weeks later, they got Julian Schwinger to come and tell us what Pauli had said. A few weeks after that, they had Ed Purcell come and tell us what Schwinger had said.''

Robert Buderi, *The Invention that Changed the World* (Simon and Schuster, New York, 1996), p. 254.